Journal of Power Sources xxx (2017) 1–7

Contents lists available at ScienceDirect

Journal of Power Sources

journal homepage: www.elsevier.com/locate/jpowsour

Part I: Electronic and ionic transport properties of the ordered and disordered $LiNi_{0.5}Mn_{1.5}O_4$ spinel cathode

Ruhul Amin [a, **], Ilias Belharouk [a, b, *]

[a] Qatar Environment and Energy Research Institute, Hamad Bin Khalifa University, Qatar Foundation, Doha, Qatar
[b] College of Science & Engineering, Hamad Bin Khalifa University, Qatar Foundation, Doha, Qatar

HIGHLIGHTS

- Synthesis of impurity free ordered and disordered $LiNi_{0.5}Mn_{1.5}O_4$ spinel.
- Measurement of ionic and electronic transport properties of $LiNi_{0.5}Mn_{1.5}O_4$.
- Determination of ionic diffusivity as function of lithium content and temperature.
- Determination of activation energies using ion and electron blocking cell configurations.

GRAPHICAL ABSTRACT

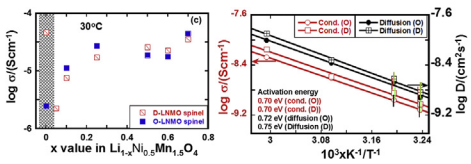

ARTICLE INFO

Article history:
Received 22 December 2016
Received in revised form
24 January 2017
Accepted 18 February 2017
Available online xxx

Keywords:
$LiNi_{0.5}Mn_{1.5}O_4$
Ordered spinel
Disordered spinel
Electronic conductivity
Ionic conductivity
Ionic diffusivity

ABSTRACT

Here, we report on the electronic and ionic conductivity and diffusivity of the ordered ($P4_332$) and disordered ($Fd\bar{3}m$) $LiNi_{0.5}Mn_{1.5}O_4$ spinel material, which have been determined by using ion and electron blocking cell configurations as a function of lithium concentration and temperature. The disordered phase exhibits about fifteen-time higher electronic conductivity than the ordered phase at room temperature in the lithiated state. Upon delithiation, the electronic conductivity of the ordered $LiNi_{0.5}Mn_{1.5}O_4$ phase increases and reaches the same levels observed for the disordered phase. The ionic conductivity and diffusivity of $LiNi_{0.5}Mn_{1.5}O_4$, in the ordered and disordered forms, are in the range of ~1×10^{-9} S/cm and ~5×10^{-9} cm^2/s, respectively. Both phases exhibit similar activation energies for the ionic conductivity and diffusivity, i.e. 0.70 ± 0.2eV and 0.74 ± 0.2eV, respectively. It can be concluded from the obtained results that the electrochemical performance of $LiNi_{0.5}Mn_{1.5}O_4$, whether ordered or disordered, is limited by lithium transport, but is fast enough to allow charge/discharge of micron-scale particles at practical C-rates.

1. Introduction

The deployment of rechargeable lithium ion batteries with higher power density, longer cycle life and improved safety in electric vehicles and grid storage applications made big strides despite several weaknesses such as the insufficient energy density of available cathode materials [1]. However, the high-voltage spinel $LiNi_{0.5}Mn_{1.5}O_4$ (labeled LNMO) is a very promising cathode material should the battery scientific community addresses the issues associated with the high voltage of the material [2–6]. The major hurdle to take care of before enabling $LiNi_{0.5}Mn_{1.5}O_4$ is the electrode/electrolyte side reactions which occur because of the insufficient electrochemical stability of available non-aqueous electrolytes [1,7]. While one may find particle size downsizing of

DOI of original article: http://dx.doi.org/10.1016/j.jpowsour.2017.02.070.
* Corresponding author. Qatar Environment and Energy Research Institute, Hamad Bin Khalifa University, Qatar Foundation, Doha, Qatar.
** Corresponding author.
E-mail addresses: mdruhul@hbku.edu.qa (R. Amin), ibelharouak@hbku.edu.qa (I. Belharouk).

http://dx.doi.org/10.1016/j.jpowsour.2017.02.071
0378-7753/

cathode materials a useful approach to enhance rate performance, the caveat is the further promotion of parasitic reactions due to increase in the surface area exposed to high voltage in the case of $LiNi_{0.5}Mn_{1.5}O_4$ [8,9]. To reduce the undesired effects of these side reactions, one needs to develop a high voltage cathode with optimal particle size distribution that does not jeopardize rate capability, energy density and battery life.

$LiNi_{0.5}Mn_{1.5}O_4$ exists in two crystallographically distinct polymorphs, i.e. face-centered cubic phase with the space group $Fd\bar{3}m$ and primitive cubic phase with the space group $P4_332$. In the face-centered and disordered structure (labeled D-LNMO), the manganese and nickel ions are randomly distributed over the 16*d* site. In the primitive cubic and ordered structure (labeled O-LNMO), the manganese and nickel ions are ordered on the 4*a* and 12*d* sites, respectively [10–12]. It has been reported that D-LNMO can be obtained either by oxygen deficiency ($LiNi_{0.5}Mn_{1.5}O_{4-\delta}$) or by nickel deficiency ($LiNi_{0.5-x}Mn_{1.5+x}O_4$) during the synthesis of the material [13–15]. In both cases, the disordered spinel phase contains trivalent ions Mn^{3+} due to charge compensation. In $LiNi_{0.5-x}Mn_{1.5+x}O_4$, impurities such as (NiO, Li_xNiO_2) having a rock salt structure were reported to form during heat treatment [14]. The Li^+ ions diffusion pathway in $LiNi_{0.5}Mn_{1.5}O_4$ is a three-dimensional network in which the ions move from one tetrahedral site to the neighboring site through vacant octahedral sites [16–19]. The activation barrier of migration is greatly influenced by the electrostatic repulsion of nearest transition metals. A theoretical study shows that the activation barrier for the migration of Li^+ ion in O-LNMO can be as low as 300 meV, which corresponds to lithium ion diffusivity of 10^{-8}-10^{-9} cm^2/s according to first-principle calculations [20].

The charge-discharge behaviors of O-LNMO and D-LNMO have been reported by several research groups [2–6]. However, the relationship structure/property and cycling performance remains a matter of controversy [2–6]. Indeed, it has been reported without a solid proof that the disordered spinel D-LNMO exhibits superior cycling performance compared to the ordered spinel O-LNMO under high C-rates [10,11]. Moreover, the ionic diffusivity results reported on $LiNi_{0.5}Mn_{1.5}O_4$ composite electrode or thin film by potentiostatic and galvanostatic intermittent titration techniques (PITT and GITT) spread over a range of several orders of magnitude (10^{-16}–10^{-9} cm^2/s) [19,21–23]. In addition, it is not clearly understood whether the rate performance of the material is limited by bulk transport properties or charge transfer reaction kinetics at the interface. The above discrepancies likely arise from the differences in the preparation of the composite electrodes, as the amount of the inactive components (carbon and binder) and degree of mixing between the electrode ingredients cannot only influence the performance of the composite electrode but also the extraction of reliable intrinsic properties of the active material.

The aim of this work is to investigate the transport properties (electronic conductivity, ionic conductivity and chemical diffusivity) and electrode-electrolyte interfacial charge transfer reaction in order to distinguish between the ordered and disordered $LiNi_{0.5}Mn_{1.5}O_4$ spinel phases and their electrochemical performances. In part (I), a systematic study, focused on the electronic conductivity, ionic conductivity and ionic diffusivity, has been conducted on pellets made of the ordered and disordered $LiNi_{0.5}Mn_{1.5}O_4$. The measurements were performed as a function of states of charge and temperatures using electron-blocking and ion-blocking cell configurations. In part (II), a complementary study on the exchange current density of the ordered and disordered $LiNi_{0.5}Mn_{1.5}O_4$ has been conducted as a function of lithium contents. In all measurements, additive-free and sintered $LiNi_{0.5}Mn_{1.5}O_4$ samples were used in order to eliminate any extrinsic effect that might be present in composite electrodes. The data obtained provide a basis for future materials optimization.

2. Experimental

2.1. Preparation of $LiNi_{0.5}Mn_{1.5}O_4$ pellets

$LiNi_{0.5}Mn_{1.5}O_4$ powder was supplied by NEI Corporation. The phase purity of the supplied powder was checked by x-ray diffraction. Pellets were prepared by pressing the powders under 340 MPa for 60s forming cylindrical samples of 14 mm in diameter. The pellets were sintered using two heat treatment procedures to obtain the ordered and disordered $LiNi_{0.5}Mn_{1.5}O_4$. In the case of the disordered $LiNi_{0.5}Mn_{1.5}O_4$ spinel (D-LNMO), the pellets were heated in air at 1000 °C for 24 h, and subsequently annealed at 725 °C for 12 h with heating and cooling rates of 10 °C/min (procedure 1); whereas in the case of the ordered $LiNi_{0.5}Mn_{1.5}O_4$ spinel (O-LNMO), the pellets were calcined at 1000 °C for 24 h followed by annealing at 650 °C for 48 h and cooling at 1 °C/min, all under argon:oxygen (1:1) atmosphere (procedure 2). These procedures yielded samples of 80–85% relative density. Higher temperatures were tried to achieve higher densities, however, the final pellets contained rock-salt impurity phases.

2.2. Electrochemical delithiation

The sintered pellets were polished to thicknesses from 0.30 to 0.80 mm. One side of the polished pellet was coated with a thin layer of carbon to ensure good electrical contact with the metal current collector in the cells. The delithiation process was performed in a Swagelok-type electrochemical cell using lithium metal foil as the counter electrode, the LNMO pellet as the working electrode, and a liquid electrolyte comprised of 1 M $LiPF_6$ dissolved in ethylene carbonate/diethyl carbonate (EC/DEC) (1:1 v/v). A Celgard membrane was used to separate the electrodes. A charging current equivalent to C/200 rate was applied using the electrochemical station Biologic (VMP3). The current was applied continuously or intermittently for one/2-h followed by a rest of two/3-h at the open circuit voltage (OCV) condition to attain steady state cell voltage. When the desired delithiated compositions were reached, the cells were disassembled and the pellets were washed with the DEC solvent, and dried at 120 °C in an inert atmosphere for 24 h. The pellets were again polished lightly on both sides to remove carbon and any surface residues. All work was conducted inside a glove box filled with argon atmosphere with less than 1 ppm oxygen and 1–2 ppm moisture content.

2.3. Electronic conductivity measurements

The ordered and disordered LNMO pellets and their delithiated forms were painted with a silver paste on both sides forming the cell configuration Ag|LNMO|Ag. The pellets were subsequently heated at 120 °C overnight in order to remove organic solvents. The Ag|LNMO|Ag cells were placed inside battery coin cell holders with support of stainless steel disks on both sides of the pellet. Direct current polarization (DC) and electrochemical impedance spectroscopy (EIS) techniques were used to measure the electrical conductivity of the samples using Biologic (VMP3) in the frequency range 2 MHz-1Hz. The measurements were performed between 25 and 100 °C using a VWR temperature controller. The sample temperatures were measured by a thermocouple placed in the proximity of the cells. The measurements were performed during both heating and cooling cycles.

Please cite this article in press as: R. Amin, I. Belharouk, Journal of Power Sources (2017), http://dx.doi.org/10.1016/j.jpowsour.2017.02.071

2.4. Ionic conductivity and diffusivity measurements

The ionic conductivity and diffusivity of the fully lithiated LNMO pellets were measured by direct current (DC) polarization/depolarization as well as electrochemical impedance spectroscopy (EIS), over the frequency range 2 MHz-10 μHz at the AC amplitude of 10 mV, as a function of temperature. Doped polyethylene oxide (PEO), which is a lithium-conducting membrane, was used as the electron-blocking electrode. The PEO membrane was fabricated by mixing PEO powder (scientific polymer products, Mw. 4,000,000) and LiI (Aldrich, 99.99%) in a 6:1 M ratio in dry acetonitrile. Preparation details can be found elsewhere [24]. The measurements were performed using the symmetric cell configuration Li|PEO|LNMO|PEO|Li in Swagelok-type cells.

2.5. X-ray diffraction and Raman spectroscopy

Powder x-ray diffraction (XRD) measurements were performed in Bragg-Brentano reflection geometry between 17 and 100° (2θ) using a Bruker D8 diffractometer and Cu-Kα radiation. Rietveld refinements were performed using the program Fullprof [25]. The backgrounds were described by linear interpolation between selected points, while pseudo-Voigt profile functions were used to fit the diffraction peaks. The unit cell parameters, profile parameters and the overall temperature factors B_{iso} were refined. As the main objective of the refinements was to extract the unit cell parameters, the structural model of $LiNi_{0.5}Mn_{1.5}O_4$ ($Fd\bar{3}m$) as published by Branford et al. was used as starting point for the refinements of all x-ray patterns [26]. The structural model ($P4_332$) was tested for the O-LNMO sample, however, it was not found to improve the agreement factors.

Raman spectra were recorded for the ordered and disordered $LiNi_{0.5}Mn_{1.5}O_4$ pellets using the Raman Microscope Kaiser Optical Hololab 5000R under the laser excitation wavelength of 785 nm.

3. Results and discussion

Fig. 1a shows the XRD patterns for the as-received $LiNi_{0.5}Mn_{1.5}O_4$ powder, the pellets sintered at 1000 °C in air and the pellets sintered at 1000 °C in ($Ar:O_2$) atmosphere according to procedures 1 and 2 (cf. experimental part). The XRD patterns show no sign of impurities after completion of the heat treatments. At first, it was not possible for us to distinguish between the ordered spinel (O-LNMO, $P4_332$) and the disordered spinel (D-LNMO, $Fd\bar{3}m$) polymorphs due to similar x-ray scattering factors of nickel and manganese. However, a careful examination of the cubic lattice parameter, as obtained by the Rietveld refinement, led us to lean to the fact that the disordered phase D-LNMO should have a slightly larger lattice parameter (8.188 Å) compared to that (8.178 Å) of the ordered phase D-LNMO because of the presence of the larger Mn^{3+} ions in D-LNMO (see Table 1).

For further confirmation, we used the Raman spectroscopy due of its sensitivity to crystal symmetry in order to distinguish between the two phases belonging to the spinel polymorphs. The Raman spectrum for the sample sintered at 1000 °C in air shows only a few broad bands, while several sharp bands are observed for the sample sintered at 1000 °C in ($Ar:O_2$) atmosphere (Fig. 1b). The presence of Raman bands around 580-620 cm^{-1} are characteristic of the symmetric stretching mode of Mn−O in the MnO6 octahedral site. The sharp peaks observed at 595 cm^{-1} and 612 cm^{-1} are attributed to the vibrational mode (F_{2g}). The splitting between these two bands clearly indicates a high degree of Mn and Ni ordering in the material treated under oxygen atmosphere, whereas the absence of the two bands (595 cm^{-1} and 612 cm^{-1})

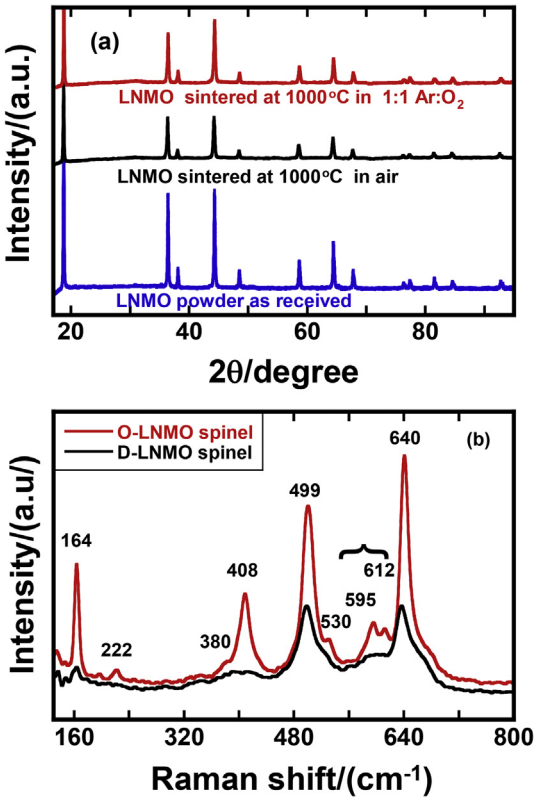

Fig. 1. a. XRD data of $LiNi_{0.5}Mn_{1.5}O_4$ spinel as received (blue), sintered at 1000 °C in air (black) and at 1000 °C in argon and oxygen atmosphere (red). b. Raman spectra of $LiNi_{0.5}Mn_{1.5}O_4$ spinel sintered at 1000 °C in air (black) and at 1000 °C in argon and oxygen atmosphere (red). (For interpretation of the references to colour in this figure legend, the reader is referred to the web version of this article.)

indicates the loss of symmetry in the material treated under air atmosphere. The Raman results obtained on both samples are in good agreement with previous reports and demonstrate that the annealing procedures used in this study effectively yield the ordered and disordered $LiNi_{0.5}Mn_{1.5}O_4$ spinel phases [27–29].

An estimation of the degree of disorder was obtained from the electrochemical charge of the $LiNi_{0.5}Mn_{1.5}O_4$ samples by measuring the extent of the voltage plateau at 4.0 V. This plateau is caused by the Mn^{3+}/Mn^{4+} redox couple and is absent in O-LNMO as shown in Fig. 2. Two mechanisms by which the high temperature sintering leads to formation of the disordered phase had been proposed, i.e. oxygen deficiency ($LiNi_{0.5}Mn_{1.5}O_{4-\delta}$) or nickel deficiency ($LiNi_{0.5-x}Mn_{1.5+x}O_4$). The latter supposes the formation of rock salt impurities as also found by others [3,13]. Since our XRD patterns did not reveal any sign of impurities we can suggest with confidence that the heat treatment at 1000 °C in air resulted in oxygen deficiencies with the formation of the disordered spinel phase $LiNi_{0.5}Mn_{1.5}O_{4-\delta}$ (D-LNMO). Fig. 2 clearly shows that the disordered spinel phase had about 4% of Mn^{3+} which corresponds to 2% of oxygen

Table 1
Lattice parameter of lithiated and partially delithiated ordered and disordered $LiNi_{0.5}Mn_{1.5}O_4$ spinel.

x in $L_{1-x}Ni_{0.5}Mn_{1.5}O_4$	Lattice parameter (Å)	
	O-LNMO spinel	D-LNMO spinel
$x = 0.00$	8.178	8.188
$x = 0.10$	8.160	8.161
$x = 0.25$	8.144	8.140

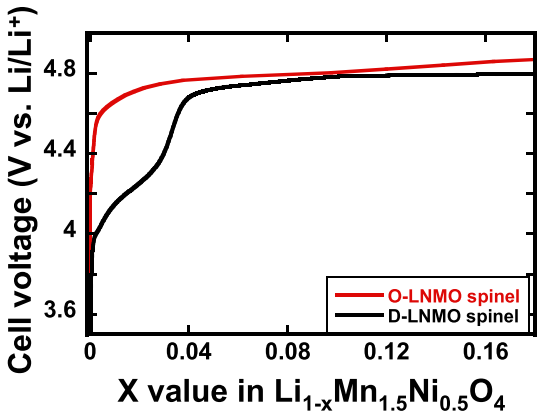

Fig. 2. Partial electrochemical delithiation of $LiNi_{0.5}Mn_{1.5}O_4$ spinel pellets performed at C/200 rate. Disordered spinel sample (black curve) and ordered spinel sample (red curve). (For interpretation of the references to colour in this figure legend, the reader is referred to the web version of this article.)

deficiency since one oxygen vacancy should be compensated by two Mn^{3+}, i.e. δ in $LiNi_{0.5}Mn_{1.5}O_{4-\delta}$ is around 0.02. The lattice parameters of the partially delithiated samples are presented in Table 1. As expected, the cubic lattice parameter of $Li_{1-x}Ni_{0.5}Mn_{1.5}O_4$ gradually decreases upon delithiation in both ordered and disordered samples (Table 1).

The temperature dependent impedance spectra of the ordered spinel O-LNMO obtained from the symmetrical cell Ag|O-LNMO|Ag are shown in Fig. 3. Nearly perfect semicircles are observed in the temperature range 25–100 °C and in the frequency range 2 MHz-1Hz. The absence of a second semicircle reveals the absence of other resistive processes and also suggests negligible ionic conductivity contribution. Note that similar shape impedance spectra were observed for all pellets whether they belong to O-LNMO or D-LNMO and their delithiated forms. The impedance spectra were simulated with an ideal equivalent resistor-capacitor (RC) circuit. The capacitance (C) values could be calculated from the fitting parameters Q and n according to the equation $C = (R^{1-n}Q)^{1/n}$, where Q is a constant phase element (CPE-T) and n is a measure of the degree of depression (CPE-P) of the impedance arc (n was found in the range of 0.98–0.94 depending upon the degree of delithiation and temperature). The derived capacitance values are in the range of 5×10^{-12} F, hence indicating that the observed impedance responses originate from the bulk (grains) of the samples and not from the grain boundaries [30]. In all samples, the absence of any additional polarization process (i.e. second semicircle) at the low frequencies indicates that the conduction is predominantly due to electronic carriers. In order to corroborate this, DC polarization and depolarization measurements were performed on O-LNMO and D-LNMO and their delithiated forms using the same cell configuration used for the EIS measurements. The current response with time is provided in the Supplementary Fig. S1 as a typical DC measurement. During the application of a constant voltage, the current increases stepwise to a constant value, and then decays stepwise when the load is off. Such a behavior is indicative of an electronically dominated conduction process. Indeed, if there was a significant contribution from ionic motion, one should expect a continuous increase of current during polarization and a similar decay of the current during depolarization with the rate constant being determined by lithium diffusion D_{Li} [31–35].

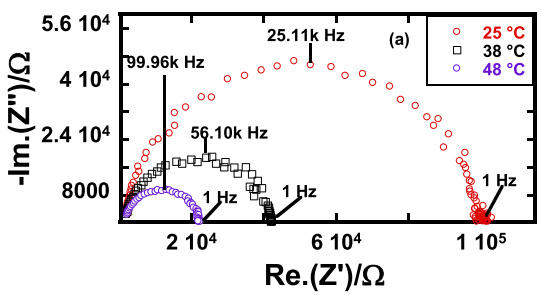

Fig. 3. Impedance spectra of ordered $LiNi_{0.5}Mn_{1.5}O_4$ spinel (O-LNMO) obtained from the ion blocking symmetrical cell configuration Ag|LNMO|Ag at increasing temperatures.

The electronic conductivities of the O-LNMO and D-LNMO samples and their delithiated forms are plotted in Fig. 4a and b as a

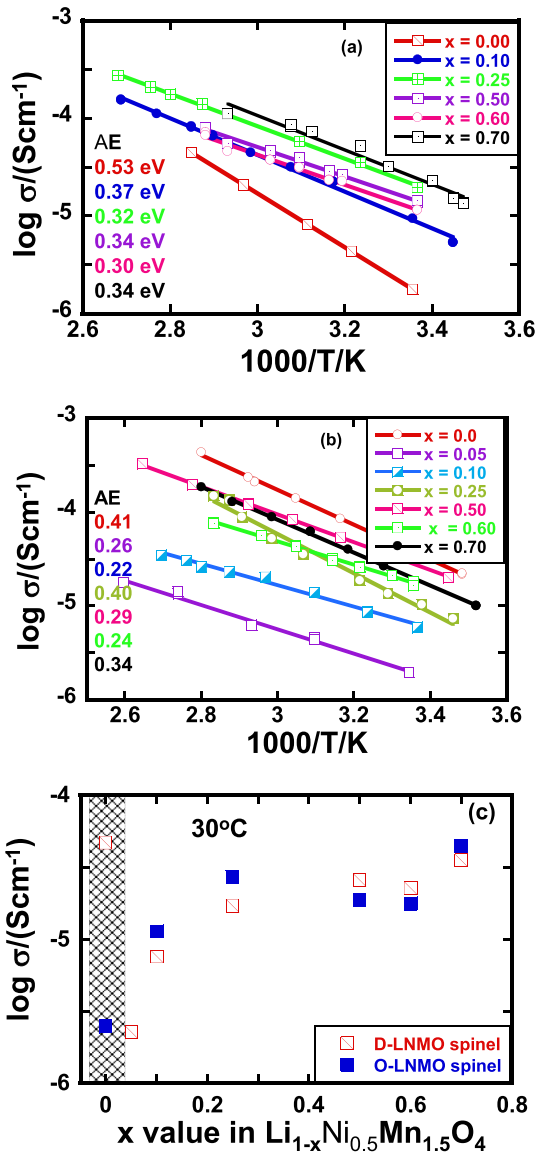

Fig. 4. a. Electronic conductivity plots of the ordered $Li_{1-x}Mn_{1.5}Ni_{0.5}O_4$ spinel as a function of inverse temperature. Legend shows the degree of delithiation and corresponding activation energies. b. Electronic conductivity plots of the disordered $Li_{1-x}Ni_{0.5}Mn_{1.5}O_4$ spinel as a function of inverse temperature. Legend shows the degree of delithiation and corresponding activation energies. c. Comparison of electronic conductivity of the ordered and disordered $Li_{1-x}Ni_{0.5}Mn_{1.5}O_4$ spinel at 30 °C. Data points are derived from the best fits of the electronic conductivity lines in Fig. 4a and b. The shaded region corresponds to the 4.0 V electrochemical plateau of the disordered spinel. Fully lithiated samples correspond to x = 0.

Please cite this article in press as: R. Amin, I. Belharouk, Journal of Power Sources (2017), http://dx.doi.org/10.1016/j.jpowsour.2017.02.071

function of the inverse of temperature. The conductivities of the ordered samples O-LNMO measured at a given temperature monotonically increase with increasing the degree of delithiation (Fig. 4c). However, on x = 0.3 and beyond, the electronic conductivity reached a level where it barely fluctuates. In contrast, the electronic conductivity of the disordered spinel D-LNMO decreased upon slight delithiation and dropped down to the level of the electronic conductivity of the lithiated ordered spinel phase. Thereafter, the electronic conductivity exhibited similar trend for both the ordered and disordered phases (Fig. 4c). Over the studied composition range, the electrical conductivity showed a thermally-activated behavior. The activation energy values, calculated using the Arrhenius law, vary from 0.53 to 0.24eV (±0.03 eV) for the O-LNMO samples and from 0.41 to 0.22eV (±0.03 eV) for the D-LNMO samples (Fig. 4a and b). The range of these values is consistent with the values reported by Kunduraci et al. for $LiNi_{0.5}Mn_{1.5}O_4$ in the ordered and disordered forms [11]. These numbers are typical values for the migration process of small polarons generally observed in mixed-valence compounds [36]. Of interest, the activation energies of the ordered spinel O-LNMO (Fig. 4a) and disordered spinel D-LNMO (Fig. 4b) are almost similar within the studied temperature range. This indicates that a similar conduction mechanism is likely taking place in both the ordered and disordered spinel materials.

O-LNMO exhibits approximately fifteen times lower electronic conductivity than the disordered D-LNMO lithiated phase (Fig. 4c). The higher electronic conductivity of D-LNMO −as compared to O-LNMO− is associated with the presence of the Mn^{3+}/Mn^{4+} mixed valence states, which leads to formation of holes in the narrow (Mn^{3+}/Mn^{4+}) band. The amount of the Mn^{3+} cations that is initially present in the disordered D-LNMO spinel gradually converts into Mn^{4+} cations upon delithiation, hence, the electronic conductivity decreases and reaches the conductivity level of the ordered O-LNMO spinel where all Mn-ions have a single valence state Mn^{4+}.

Except the lithiated D-LNMO, the electronic conductivities of the partially delithiated (x up to 0.3) samples increase with increasing of the state of charge due to the presence of Ni^{2+}/Ni^{3+} mixed valence states, and thus the creation of holes in the (Ni^{2+}/Ni^{3+}) narrow conduction band. On x = 0.3 and beyond (Fig. 4c), the electronic conductivity slightly decreases due to the complete conversion of Ni^{2+} into Ni^{3+} when x in $Li_{1-x}Ni_{0.5}Mn_{1.5}O_4$ approached 0.5. Further increase of conductivity was observed beyond x = 0.6 which is associated with the formation of the mixed valence state Ni^{3+}/Ni^{4+}. Note that we were unable to measure the conductivity beyond x = 0.7 as the pellets became very fragile due to significant lithium removal.

Fig. 5a shows the impedance plot of the ordered $LiNi_{0.5}Mn_{1.5}O_4$ material measured at 61 °C by using the cell configuration Li/PEO/O-LNMO/PEO/Li. One should note that the results obtained with the electron-blocking cells must take into account the effect of temperature on the ionic conductivity of the PEO blocking layer. Unlike the ion-blocking cells discussed above, the impedance spectra in the electron-blocking configuration consist of two semicircles followed by a Warburg response in the low frequencies region (inset, Fig. 5a). The high frequency semicircles represent the total resistance to the electronic and ionic motion including contributions from the bulk conductivity of PEO. The Warburg response is indicative of a stoichiometric polarization owing to the blocking of electrons. In order to obtain the ionic conductivity and diffusivity, the impedance spectra were fitted with the equivalent electrical circuit shown in Fig. 5b. Good agreement between the simulated and experimental data was obtained, provided that the relaxation time for ion diffusion can be obtained from the relaxation frequency according to the relationship $\tau = \frac{1}{2\pi f}$, and the ionic

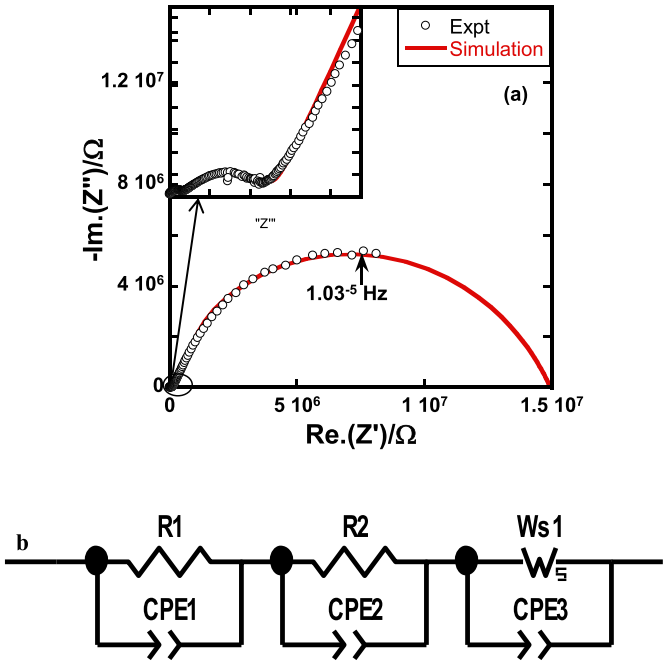

Fig. 5. a. Impedance spectrum of the ordered $LiNi_{0.5}Mn_{1.5}O_4$ spinel obtained from the electron blocking cell configuration Li|PEO|LNMO|PEO|Li at ~61 °C. Inset shows a zoom of the high frequency region. Red solid line is the simulation curve according to the equivalent circuit of Fig. 5b. b. Equivalent circuit used to evaluate the impedance spectra with the Zview program. (For interpretation of the references to colour in this figure legend, the reader is referred to the web version of this article.)

resistance can be obtained from the low frequency Warburg response (Fig. 5a). Quite similar impedance spectra were observed for both the ordered and disordered $LiNi_{0.5}Mn_{1.5}O_4$ at 61 °C, 50 °C, 40 °C and 35 °C. Impedance spectra of D-LNMO measured at 61 °C and of O-LNMO measured at three different temperatures are displayed in Figs. S2 and S3, respectively. At temperatures below 50 °C, the frequency range was not sufficiently wide to obtain the relaxation frequency. At lower temperature interval, the relaxation frequency of the impedance spectra was obtained by extrapolation of the simulated parameters (cf. Fig. S3). We were not able to measure impedance spectra beyond 61 °C due to the melting of PEO film and short circuit of the cell. Conversely, sintered LNMO pellets thicker than 0.3–0.4 mm must be used in the electron blocking cell which requires a longer waiting time (several days) at low temperatures before reaching the relaxation frequency or steady state voltage response. Therefore, we were only able to measure the activation energy for the ionic conductivity and diffusivity within the temperature window 35-61 °C. A suitable electron blocking material with wide temperature range stability and exhibiting no interfacial reaction with the active material must be found.

The temperature dependence plots of the ionic conductivity and diffusivity of the ordered and disordered $LiNi_{0.5}Mn_{1.5}O_4$ are compared in Fig. 6. The conductivity and diffusivity data at lower temperature interval are associated with minor uncertainty due to the extrapolation of fitted parameters which is shown by error bar in Fig. 6. The ionic conductivity Arrhenius relationship demonstrates that the activation energies of the ordered and disordered spinel phases are similar (0.70 ± 0.2 eV). The activation energies for the ionic diffusivity of ordered and disordered spinel phases are 0.72 ±0.2 and 0.75 ±0.2 eV, respectively. To the best of our knowledge, the above measurements provide the first set of results on the ion transport parameters of $LiNi_{0.5}Mn_{1.5}O_4$ in the form of

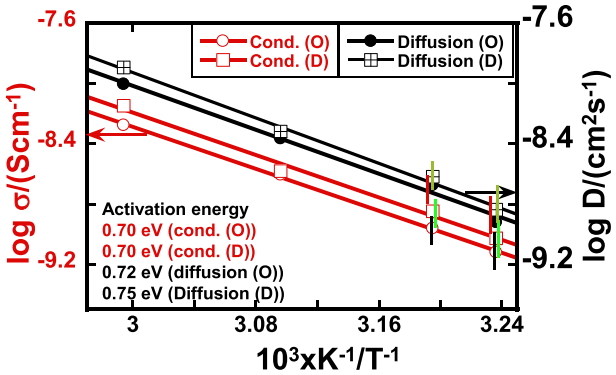

Fig. 6. Comparison of ionic conductivity and diffusivity of the ordered and disordered $LiMn_{1.5}Ni_{0.5}O_4$ spinel measured by using the electron blocking cell configuration Li|PEO|LNMO|PEO|Li. cond.(O) and cond. (D) stand for the conductivity of ordered and disordered $LiMn_{1.5}Ni_{0.5}O_4$, respectively; and diffusion(O) and diffusion(D) stand for the diffusivity of ordered and disordered $LiMn_{1.5}Ni_{0.5}O_4$, respectively.

sintered dense pellets. The obtained activation energies are comparable to those for other lithium ion cathode compounds [37,38].

Of significance, it can be seen that the ionic diffusivity is higher that the ionic conductivity within the studied temperature range (Fig. 6). Given the fact that the electronic conductivity is predominant in $LiNi_{0.5}Mn_{1.5}O_4$, the Li^+ ion diffusivity and conductivity should have the form $D_{Li} \propto \sigma_{ion}\left(\frac{x_{ion}}{c_{ion}} + \frac{x_{eon}}{c_{eon}}\right)$, where x_{ion} and x_{eon} refer to the contributions due to the trapping of ionic and electronic carriers, and c_{ion}, c_{eon} denote to the ionic and electronic carrier concentrations [39]. Since the measurements were performed at relatively higher temperatures there should be absence of charge carrier trapping effect (x_{ion} and x_{eon}). That is to say that the association-dissociation of charge carriers is not predominant in the measured temperature range. Provided that in the intrinsic dilute defect case, $c_{ion} \gg 1$, the ionic diffusivity should be higher than the ionic conductivity according to the above equation, as it is also observed in Fig. 6.

Thereafter, DC polarization/depolarization measurements were also performed using the same electron blocking cell setup in order to compare with the result obtained from the impedance measurements. These measurements were not performed at low temperatures due to the excessively long time required to reach the steady state. Fig. 7a shows the time dependence of the polarization/depolarization voltage curve measured at 50 °C. On application of a constant load (6.8×10^{-2} mA), the voltage immediately jumped from zero to $IR_{el}R_{ion}/(R_{el} + R_{ion})$, where R_{ion} and R_{el} are the resistances due to Li^+ ion and electronic carriers. With increasing the time, the partial electronic current decreases and eventually vanishes due to the blocked electrons. A steady state is then observed (voltage being IR_{ion}) during which the total current is carried only by the non-blocked ions. The relaxation time of the polarization process is τ, which provides the chemical diffusion D_{Li} (via $\tau = L^2/(\pi^2 D_{Li})$. The ionic conductivity is obtained from the ionic resistance by measuring the polarization/depolarization cell voltage on the application of a constant current. It should be noted that owing to the internal concentration profiles, σ_{ion} and D_{Li} are averaged over a lithium composition range, corresponding to a polarization voltage of 250 mV. The behavior of the depolarization was analogous to that during polarization. Owing to the relatively high diffusion coefficients, a steady state cell voltage was reached during the polarization at ~50 °C. The long-time polarization voltage ($t > \tau$) depends on time according to the following equation [31–33]:

$$\ln\left(U_{(t)} - U_{(t=\infty)}\right) = \ln A + \frac{8}{\pi^2}\frac{t}{\tau} \quad (1)$$

where A is the constant term for a particular material, $U_{(t)}$ and $U_{(t=\infty)}$ are the cell voltage at time t and $t_{(\infty)}$, respectively. A plot of ln ($|U(t)-U(t=\infty)|$) vs. t should generate a straight line with a slope of $\tau \propto \left(\frac{1}{D_{Li}}\right)$, as indicated in Fig. 7b. Details discussion about the equation and data evaluation will be found elsewhere [34,35,38]. The diffusivity and ionic conductivities data derived from the DC measurements are presented in Table 2 and compared with the AC data at 50 °C, which demonstrates a good agreement between these results obtained on both the ordered and disordered $LiNi_{0.5}Mn_{1.5}O_4$ (Table 2).

It should be mentioned that the disordered spinel $LiNi_{0.5}Mn_{1.5}O_{4-\delta}$ had been reported to exhibit better rate capability than its ordered counterpart [10,11]. While previous reports suggested that this may be the result of a better bulk transport in the disordered structure, our results clearly demonstrate that neither a

Table 2
Comparison of ionic conductivity and diffusivity of the ordered and disordered $LiNi_{0.5}Mn_{1.5}O_4$ samples measured at ~50 °C obtained from AC and DC measurements.

Ionic conductivity σ_{ion} (Scm^{-1})		Ionic Diffusivity D (cm^2/s)		Technique used
D-LNMO	O-LNMO	D-LNMO	O-LNMO	
$\sim 5 \times 10^{-9}$	$\sim 4 \times 10^{-9}$	$\sim 8 \times 10^{-9}$	$\sim 6 \times 10^{-9}$	DC
$\sim 3 \times 10^{-9}$	$\sim 2 \times 10^{-9}$	$\sim 5 \times 10^{-9}$	$\sim 4 \times 10^{-9}$	AC

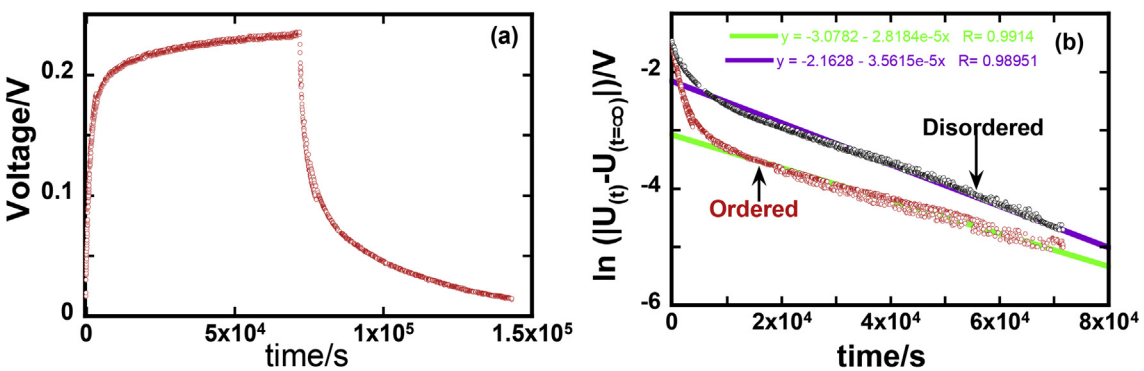

Fig. 7. (a) Typical polarization/depolarization cell voltage with time under constant applied current on the electron blocking Li|PEO|O-LNMO|PEO|Li cell configuration at ~50 °C for the ordered $LiNi_{0.5}Mn_{1.5}O_4$ spinel, and (b) fitting of the polarization cell voltage for the ordered and disordered $LiNi_{0.5}Mn_{1.5}O_4$.

difference in electronic conductivity nor lithium ion diffusivity can explain the electrochemical performance of the two polymorphs. With these ruled out, it is likely that the difference in rate capability may be due to morphological impacts.

4. Conclusion

The electronic conductivity and ionic conductivity and diffusivity of $Li_{1-x}Ni_{0.5}Mn_{1.5}O_4$ having the ordered and disordered spinel structures have been measured as a function of lithium content and temperature. No major differences were observed in the transport properties of $LiNi_{0.5}Mn_{1.5}O_4$, whether ordered and disordered, except for the higher electronic conductivity of the disordered phase in the lithiated state. The lithium ion conductivity and diffusivity measured at 50 °C on the ordered and disordered $LiNi_{0.5}Mn_{1.5}O_4$ spinel are around in the order of 1×10^{-9} Scm^{-1} and ~5×10^{-9} cm^2s^{-1}, respectively; and the activation energies are in the range of 0.70eV ± 0.2 and 0.74eV ± 0.2, respectively. From the magnitude of the electronic and ionic transport parameters across the range of lithium concentration and temperature, it can be concluded that the chemical diffusion is limited by lithium ion transport rather than electronic conductivity in both the ordered and disordered $LiNi_{0.5}Mn_{1.5}O_4$, and that the bulk transport is rapid enough to allow charging and discharging of micron size particles at practical C-rates.

Acknowledgments

We would like acknowledge Prof. Yet-Ming Chiang of Massachusetts Institute of Technology (MIT) for allowing us to use his facilities to carry out a part of this work. This work was supported by the Assistant Secretary for Energy Efficiency and Renewable Energy, Office of Vehicle Technologies of the U.S. Department of Energy under Contract No. DE-AC02-05CH11231, Subcontract No. 6920899 under the Batteries for Advanced Transportation Technologies (BATT) Program.

Appendix A. Supplementary data

Supplementary data related to this article can be found at http://dx.doi.org/10.1016/j.jpowsour.2017.02.071.

References

[1] E. Vinodkumar, M. Rotem, E. Ran, S. Gregory, D. Aurbach, Energy Environ. Sci. 4 (2011) 3243–3262.
[2] K. Amine, H. Tukamoto, H. Yasuda, Y. Fujita, J. Electrochem. Soc. 143 (1996) 1607–1613.
[3] Q.M. Zhong, A. Bonakdarpour, M.J. Zhang, Y. Gao, J.R. Dahn, J. Electrochem. Soc. 144 (1997) 205–213.
[4] H.F. Xiang, X. Zhang, Q.Y. Jin, C.P. Zhang, C.H. Chen, X.W. Ge, J. Power Sources 183 (2008) 355–360.
[5] H.M. Wu, I. Belharouak, H. Deng, A. Abouimrane, Y.K. Sun, K. Amine, J. Electrochem. Soc. 156 (2009) A1047–A1050.
[6] J. Hassoun, S. Panero, P. Reale, B. Scrosati, Adv. Mater. 21 (2009) 4807–4810.
[7] J.B. Goodenough, Y. Kim, Chem. Mater. 22 (2010) 587–603.
[8] Y. Talyosef, B. Markovsky, R. Lavi, G. Salitra, D. Aurbach, D. Kovacheva, M. Gorova, E. Zhecheva, R. Stoyanova, J. Electrochem. Soc. 154 (2007) A682–A691.
[9] J. Cabana, H. Zheng, A.K. Shukla, C. Kim, V.S. Battaglia, M. Kunduraci, J. Electrochem. Soc. 158 (2011) A997–A1004.
[10] J.H. Kim, S.T. Myung, C.S. Yoon, S.G. Kang, Y.K. Sun, Chem. Mater. 16 (2004) 906–914.
[11] M. Kunduraci, G.G. Amatucci, J. Electrochem. Soc. 153 (2006) A1345–A1352.
[12] M. Kunduraci, G.G. Amatucci, J. Power Sources 165 (2007) 359–367.
[13] D. Pasero, N. Reeves, V. Pralong, A.R. West, J. Electrochem. Soc. 155 (4) (2008) A282–A291.
[14] J. Cabana, M. Casas-Cabanas, O.N. Omenya, A. Chernova, D. Zeng, M.S. Whittingham, C.P. Grey, Chem. Mater. 24 (2012) 2952–2964.
[15] Z. Moorthead-Rosenberg, D.W. Shin, K.R. Chemelewski, A. Manthiram, Appl. Phys. Lett. 100 (2012) 213909–213914.
[16] B. Ammunden, J. Roziere, M.S. Islam, J. Phys. Chem. B 101 (1997) 8156–8163.
[17] M. Wakihara, Electrochem. (Tokyp Jpn. 73 (2005) 328–335.
[18] L. Eunseok, K.A. Person, Energy Environ. Sci. 5 (2012) 6047–6052.
[19] H. Xia, Y.S. Meng, L. Lu, G. Ceder, J. Electrochem. Soc. 154 (8) (2007) A737–A743.
[20] X. Ma, B. Kang, G. Ceder, J. Electrochem. Soc. 157 (8) (2010) A925–A931.
[21] D. Kovacheva, B. Markovsky, G. Salitra, Y. Talyosef, M. Gorova, E. Levi, M. Riboch, H.-J. Kim, D. Aurbach, Electrochim. Acta 50 (2005) 5553–5560.
[22] M. Mohamedi, M. Makino, K. Dokko, T. Itoh, I. Uchid, Electrochim. Acta 48 (2002) 79–84.
[23] K.M. Shaju, G.V. Subba Rao, B.V.R. Chowdari, J. Mater. Chem. 13 (2003) 106–113.
[24] Y. Liu, S. Gorgutsa, C. Santato, M. Skorobogatiy, J. Electrochem. Soc. 159 (4) (2012) A349–A356.
[25] J. Rodriguez-Carvajal, Fullprof Suite, LLB Sacley & LCSIM Rennes, France, 2003.
[26] W. Branford, M.A. Green, D.A. Neumann, Chem. Mater 14 (2002) 1649–1656.
[27] K. Saravanan, A. Jarry, R. Kostcki, G. Chen, A study of room-temperature LixMn1. 5Ni0. 5O4 solid solutions, Sci. Rep. 5 (2015).
[28] Y. Wei, K.-B. Kim, G. Chen, Electrochim. Acta 51 (2006) 33653373.
[29] M. Kundurci, G.G. Amtucci, J. Power Sources 165 (2007) 359–367.
[30] F.S. Baumann, Oxygen Reduction Kinetics on Mixed Conducting SOFC Model Cathodes, PhD thesis, Stuttgart University press, 2006, p. 33.
[31] C. Wagner, Proc. 7th Meeting of the Intern. Committee on Electrochem. Thermodyn. & Kinetics, Lindau, 1955.
[32] I. Yokota, J. Phys. Soc. Jpn. 16 (1961) 2213–2223.
[33] J. Maier, Physical Chemistry of Ionic Materials: Ions and Electrons in Solids, Wiley, Chichester, 2004.
[34] R. Amin, P. Balaya, J. Maier, Electrochem. Solid-State Lett. 10 (1) (2007) A13–A16.
[35] R. Amin, C. Lin, T. Maier, J. Phys. Chem. Chem. Phys. 10 (2008) 3519–3523.
[36] T. Maxisch, F. Zhou, G. Ceder, Phys. Rev. B 73 (2006) 104301.
[37] R. Amin, J. Maier, P. Balaya, D.P. Chen, C.T. Lin, Solid State Ionics 178 (2008) 1683–1687.
[38] A.K. Ivanov-Shitz, V.V. Kireev, O.K. Mel'nikov, L.N. Demianets, Crystallogr. Rep. 46 (2001) 864–867.
[39] J. Maier, J. Am. Ceram. Soc. 76 (1993) 1212–1217.